J Biol Inorg Chem (2005) 10: 778–789
DOI 10.1007/s00775-005-0026-0

ORIGINAL ARTICLE

Christopher R. Kinsinger · Benjamin F. Gherman
Laura Gagliardi · Christopher J. Cramer

How useful are vibrational frequencies of isotopomeric O_2 fragments for assessing local symmetry? Some simple systems and the vexing case of a galactose oxidase model

Received: 28 June 2005 / Accepted: 23 August 2005 / Published online: 27 September 2005

Abstract The tendency for mixed-isotope O_2 fragments to exhibit different stretching frequencies in asymmetric environments is examined with various levels of electronic structure theory for simple peroxides and peroxyl radicals, as well as for a variety of monocopper–O_2 complexes. The study of the monocopper species is motivated by their relevance to the active site of galactose oxidase. Extensive theoretical work with an experimental model characterized by Jazdzewski et al. (*J. Biol. Inorg. Chem.* 8:381–393, 2003) suggests that the failure to observe a splitting between $^{16}O^{18}O$ and $^{18}O^{16}O$ isotopomers cannot be taken as evidence against end-on O_2 coordination. Conformational analysis on an energetic basis, however, is complicated by biradical character inherent in all of the copper–O_2 singlet structures.

Keywords Copper superoxide · Copper peroxide · Raman spectroscopy · Galactose oxidase · Density functional theory

Introduction

The binding of molecular oxygen in mononuclear copper oxidases [1, 2], such as galactose oxidase [3, 4] and amine oxidase [5, 6], and in noncoupled binuclear monooxygenases such as dopamine β-monooxygenase [7] and peptidylglycine α-amidating monooxygenase [8–12] is a crucial step in these enzymes' catalytic mechanisms. Of particular interest has been ascertaining the binding mode of dioxygen to the Cu center and differentiating between end-on (η^1) and side-on (η^2) coordination. Numerous biomimetic model complexes have been designed in order to facilitate characterization of the 1:1 copper–dioxygen adducts formed in these enzymes [13, 14]. Experimental challenges, namely, that such complexes are typically short-lived, highly reactive with a tendency to dimerize, and difficult to crystallize, have complicated these efforts. Resonance Raman (RR), UV–vis, and electron paramagnetic resonance spectroscopies have therefore become the tools of choice for studying Cu–O_2 complexes [14].

RR in particular has shown its utility in assigning 1:1 Cu–O_2 adducts as superoxo or peroxo in character [14]. Typical values for O–O stretching frequencies of 1,075–1,200 cm^{-1} for superoxo ligands and 790–930 cm^{-1} for peroxo ligands are well established [15, 16] and make such an approach practical. For example, a $\nu(^{16}O–^{16}O)$ frequency of 1,122 cm^{-1} was used to identify a 1:1 Cu–O_2 species supported by a tris(2-dimethylaminoethyl)amine ligand as a superoxo complex (**1**, Structure 1) [17]. A different Cu–O_2 complex **2** with the tridentate ligand HB(3-*t*-Bu-5-*i*Prpz)$_3$ had a RR peak at 1,112 cm^{-1} for the $^{16}O–^{16}O$ vibration, supporting its assignment as a superoxo species as well [18, 19].

In addition, RR studies of *isotopically labeled* 1:1 Cu–O_2 adducts may in principle offer a means to differentiate between η^1 and η^2 coordination modes. End-on coordination might reasonably be expected to result in different values for mixed-isotope $^{16}O–^{18}O$ stretching frequencies depending upon which of the two oxygen atoms is coordinated to the metal. Side-on coordination, on the other hand, would be expected to result in equal or very nearly equal stretching frequencies for the two singly labeled isotopomers given the locally symmetric nature of the coordination. While this idea is clear in principle, its utility in practice has been limited: isotopomer peak splitting has only rarely been reported with

Electronic Supplementary Material Supplementary material is available for this article at http://dx.doi.org/10.1007/s00775-005-0026-0.

C. R. Kinsinger · B. F. Gherman · C. J. Cramer (✉)
Department of Chemistry and Supercomputer Institute, University of Minnesota, 207 Pleasant St. SE, Minneapolis, MN 55455, USA
E-mail: cramer@chem.umn.edu
Tel.: +1-612-6240859
Fax: +1-612-6262006

L. Gagliardi
Department of Physical Chemistry, "F. Accascina" University of Palermo, Viale delle Scienze, Parco d'Orleans II Pad 17, 90128 Palermo, Italy

certainty. The "classic" example is oxyhemerythrin, where mixed-isotope peaks were not resolved, but deconvolution of a flattened, broadened absorption band led to an assignment of isotopomeric absorptions separated by 5 cm^{-1} and having widths at half height of 5.5 cm^{-1} [20, 21] (the O_2 fragment in this case is protonated, i.e., it is a hydroperoxo ligand [22], although this was not known at the time of the original experiment). In other examples, cobalt(tetramesitylporphine)superoxide **3** has been assigned [23] to exhibit a separation between isotopomers of about 11 cm^{-1} in ν(O–O) (the splitting is approximate since both O–O stretching bands are observed as shoulders on a porphyrin absorption) and a broad mixed-isotope band for $Pd(O_2)(t\text{-BuNC})_2$ in an oxygen matrix has been resolved into two peaks separated by 4–5 cm^{-1} [24]. A more ambiguous application of the isotopomer principle was reported by Chaudhuri et al. [25] for a copper complex supported by an iminosemiquinone **4** in which they observed a broad, mixed-label band at 939 cm^{-1} and assigned it to the superposition of two individual isotopomer bands at 932 and 942 cm^{-1}. With such rare examples of isotopomer peak splitting, an important question is whether such peak splitting or the absence thereof (i.e., the negative result) is sufficient to differentiate between η^1 and η^2 coordination modes.

Schatz et al. [26] recently faced this exact question for the case of a 1:1 Cu–O_2 adduct with a tris(tetramethylguanidino)tren ligand **5**. The RR spectrum showed only a single absorption for the two mixed-label isotopomers, which might be interpreted to imply a side-on coordination mode. However, frequencies calculated at the density functional level for structures optimized with η^1 and η^2 coordination modes were predicted in *both* cases to be independent of isotopomerism. On the basis of computed relative energies and all of the frequency data, Schatz et al. concluded that the coordination mode was end-on. However, interpretation of density functional results in such systems can be complicated by the varying degrees of multiconfigurational character that 1:1 Cu–O_2 adducts may exhibit both intrinsically and as a function of coordination motif [27–29]. This variation can lead to significant errors in computed energies and, in principle, vibrational force constants.

Our own interests in this area were piqued by recent work of Jazdzewski et al. [30], who reported the synthesis of a 1:1 Cu–O_2 galactose oxidase model complex **6** supported by a ligand composed of a 2,4-di-*tert*-butylphenolate linked at N1 to a 4,7-diisopropyl-1,4,7-triazacyclononane. A crystal structure was not obtained for **6**. On the basis of UV–vis and RR spectroscopy, including in the latter case a failure to observe mixed-isotope splitting, Jazdzewski et al. tentatively assigned the structure to have a side-on bound oxygen oriented orthogonally to the apically situated phenoxide (Structure 1).

In the process of studying **6**, we devoted considerable effort to assessing the sensitivity of O–O stretching frequencies to asymmetric isotopic substitution. This work reports the results of those studies on simple model systems ROO• and ROOH, where R is a halogen. For these cases, some experimental data are available and several different levels of electronic structure theory can be conveniently brought to bear. We additionally examine various structural and theoretical analogs of **6** to assess this same sensitivity. Finally, we report on the

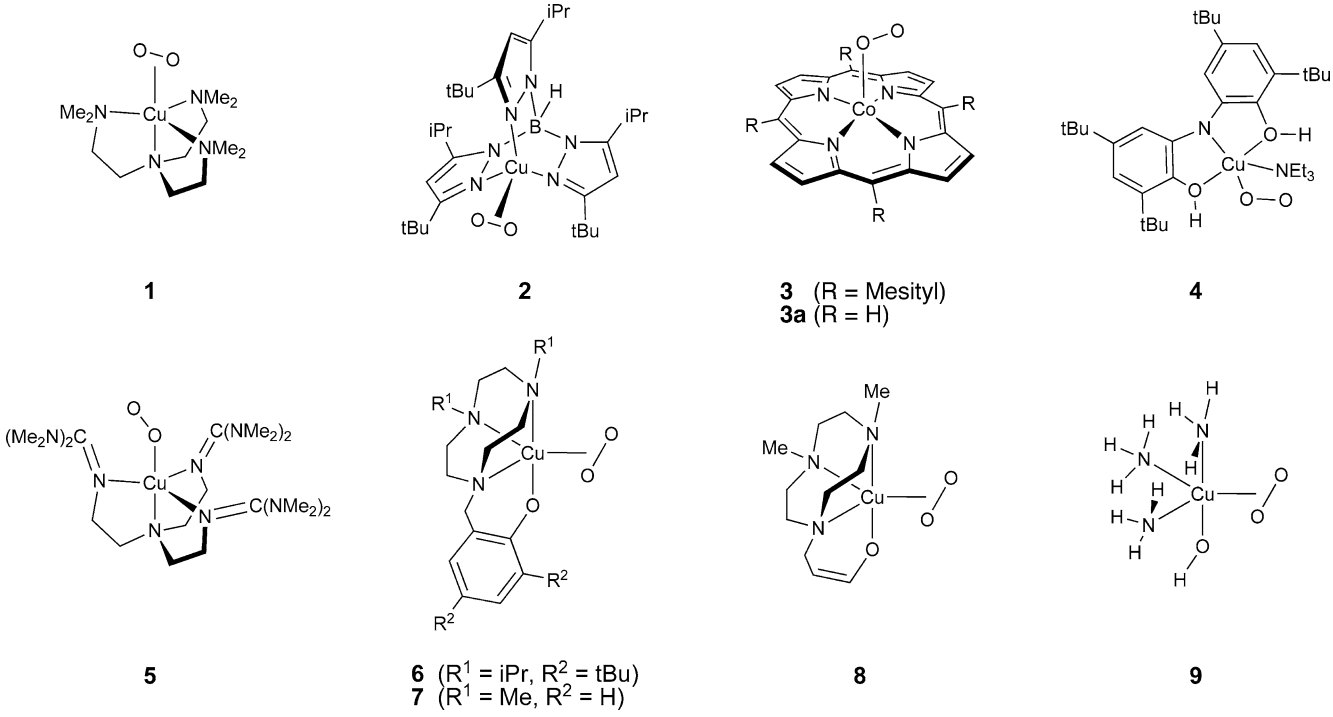

Structure 1

ability of theoretical techniques to settle the vexing question of the structure of **6** on the basis of energetic and spectral predictions.

Theoretical methods

Calculations on ROOH and ROO• molecules (R is F, Cl, Br, I) employed the 6-31G(2df,p) basis set [31] on all atoms except for Br and I, for which the Stuttgart/Dresden effective core potential basis set [32] was used. All structures were fully optimized and vibrational frequencies were computed within the harmonic oscillator approximation [33] at three different levels of theory: density functional theory (DFT) using the *m*PWPW91 [34–36] generalized gradient approximation, second-order perturbation theory (MP2) [37], and coupled-cluster theory including all single and double excitations [38] from the Hartree–Fock (HF) reference. Unrestricted wave functions [33] were used for the open-shell ROO• cases.

For **6** and most of its analogs (vide infra), structures were optimized at the *m*PWPW91 level for both singlet and triplet spin states. Singlet states were optimized both with restricted and with unrestricted, broken-symmetry formalisms. The basis set consisted of the CEP-31G effective-core-potential basis on Cu [39], the 6-311G(d) basis set [31] on the ligand heteroatoms and O_2, the 6-31G basis set [31] on carbon atoms, and the STO-3G basis set [31] on hydrogen atoms. This functional/basis-set combination was chosen on the basis of its prior good performance in the computation of O–O stretching frequencies in various metal–oxygen complexes [27]. In select instances, additional calculations were performed with the B3LYP [40–43] functional.

One key analog, **7**, was constructed by replacing the isopropyl groups in **6** with methyl groups and removing the *t*-butyl groups from the aromatic ring. In the case of the isopropyl groups, each deleted methyl group was replaced by a hydrogen atom aligned along the C–C bond and having a bond length of 1.1 Å. In the case of the *t*-butyl groups, each deleted group was replaced by a hydrogen atom aligned along the C–C bond and having a bond length of 1.09 Å. Geometries of **7**, varying one from another depending on the theoretical model and spin state, were always held frozen in subsequent calculations.

A slightly smaller analog, **8**, additionally removed all of the atoms of the aromatic system in **7** other than the three connecting the phenoxide oxygen to the triazacyclononane nitrogen (Structure 1). In order to vary the geometry of O_2 coordination in **8**, structures were fully optimized for several different choices of nuclear charges on the nitrogen atoms of the ligand, in particular, nitrogen nuclear charges were assigned values between 6 and 8 (where 7 is, of course, the physically observed value). While such structures obviously have no *chemical* relevance, they are useful to the extent that they generate stationary points having different coordination geometries for oxygen in an otherwise minimally changed formal environment. Such stationary points are then appropriate for computation of vibrational frequencies. In addition, partial optimizations of **8** (with "normal" nuclear charges) were carried out constraining the Cu–O–O angle to various values; for these structures, O–O stretching frequencies were computed after projecting out the influence of the constrained coordinate.

To more accurately assess energetics, we employed second-order perturbation theory from multiconfigurational reference wave functions (CASPT2) [44]. In this case, single-point energies were computed for geometries of **7**, and also for frozen geometries of **9**, where **9** was constructed by deleting all hydrogen atoms from **7** and all carbon atoms not attached to heteroatoms. The remaining carbon atoms were then changed to hydrogen atoms with bond lengths to their respective heteroatoms shortened to 1.0 Å (i.e., the hydrogen atoms point along the original bond vectors) and again single-point energies were computed. Three different basis sets/computational protocols were examined. In one set of calculations, a Stuttgart effective core potential was used on the Cu atom [45]. The accompanying basis set for the 19 valence electrons was contracted to 6s5p3d. For the other atoms, basis sets of atomic natural orbital (ANO) type were used [46]. For N and O a primitive set of 10s6p3d was contracted to 3s2p1d, while for H a primitive set of 7s3p was contracted to 2s [47]. We shall refer to this basis set as BS1.

In a second set of calculations, relativistic all-electron atomic basis sets of ANO type were used for *all* atoms [46]. For Cu a primitive set of 21s15p10d6f4g2h functions was contracted/truncated to 6s5p3d2f. For O and N a primitive set of 14s9p4d3f2g was contracted/truncated to 4s3p2d, and for H a primitive set of 8s4p3d1f was contracted/truncated to 2s1p [47]. We shall refer to this basis set as BS2. In this set of calculations scalar relativistic effects were taken into account using the second-order Douglas–Kroll–Hess Hamiltonian. The scalar part of this Hamiltonian was used in the generation of the complete-active-space self-consistent-field (CASSCF) wave function. Spin–orbit coupling was not included since it is reasonable to assume that such an effect will be negligible in this system.

The third set of calculations mimicked the second, except that the set of Cu primitives in BS2 was contracted to 5s4p2d1f, the basis functions for N and O were those of BS1, and the basis functions for H contracted the primitives of BS1 to a single s function. For calculations on **7**, a primitive set of 10s6p3d was contracted/truncated to 3s2p for C. This basis set, which we call BS3, is quite similar to that used for all of the DFT calculations, except that an all-electron basis is used for Cu in place of a core potential.

In the case of **9**, various choices of complete active spaces [48] ranging in size from (6,6) to (12,12) were surveyed within the context of the different basis sets and the results are discussed more completely later. Choice of active space was complicated by the degree

Table 1 Isotopomeric O–O vibrational frequencies (cm^{-1}) for ROOH molecules

Molecule	Theory[a]	$\nu(H^{18}O^{16}OR)$	$\nu(H^{16}O^{18}OR)$	$\Delta\nu$
HOOF	DFT	967.4	964.9	2.5
	MP2	985.0	980.0	5.0
	CCSD	997.4	992.4	5.0
HOOCl	DFT	863.3	865.1	−1.8
	MP2	863.1	865.8	−2.7
	CCSD	907.0	908.6	−1.6
HOOBr	DFT	914.9	918.2	−3.3
	MP2	870.1	873.4	−3.3
	CCSD	912.8	915.2	−2.4
HOOI	DFT	893.7	897.4	−3.7
	MP2	861.8	864.9	−3.1
	CCSD	906.5	909.0	−2.5

Optimized geometries and homoisotopic vibrational frequencies may be found in supporting information
[a]See "Theoretical methods" for model and basis set details

to which aromatic π orbitals and Cu- and O_2-based orbitals were prone to mixing. Thus, it is not possible to describe most of these orbitals as being well-localized hybrids. However, by the time the active space had been expanded to (12,12) by including progressively lower energy occupied and higher energy virtual orbitals, the occupation numbers of three of the occupied orbitals were 1.96 or greater and those for three of the virtuals were 0.02 or smaller, suggesting that this active space includes the most important orbitals necessary for accounting for nondynamical correlation. On the basis of our analysis, we then carried out computations on **7** using only the (12,12) active space and BS3.

Finally, an analog of **3** was computed in which the mesityl substituents on the porphyrin ring were replaced with H atoms (**3a**). The same level of DFT theory and basis set choice was made for **3a** as for optimizations of **6**.

All *m*PWPW91 (hereafter referred to simply as DFT), B3LYP, MP2, and CCSD calculations were carried out using Gaussian03 [49]. All CASSCF and CASPT2 calculations were carried out using MOLCAS6.2 [47].

Table 2 Isotopomeric O–O vibrational frequencies (cm^{-1}) for ROO• molecules

Molecule	Theory[a]	$\nu(\bullet^{18}O^{16}OR)$	$\nu(\bullet^{16}O^{18}OR)$	$\Delta\nu$
•OOF	DFT	1,456.5	1,457.2	−0.7
	MP2	1,291.4	1,292.8	−1.4
	CCSD	1,398.2	1,400.5	−2.3
	Expt.	1,449[b], 1,453[c]	1,449[b], 1,453[c]	0.0
•OOCl	DFT	1,396.3	1,398.4	−2.1
	MP2	1,093.2	1,091.5	1.7
	CCSD	1,290.7	1,295.8	−5.1
	Expt.[d]	1,400.1	1,402.3	−2.2
•OOBr	DFT	1,409.2	1,410.9	−1.7
	MP2	1,022.4	1,016.3	6.1
	CCSD	1,379.2	1,383.5	−4.3
	Expt.[e]	1,445.7	1,445.7	0.0
•OOI	DFT	1,388.7	1,390.6	−1.9
	MP2	1,695.7	1,699.4	−3.7

Optimized geometries and homoisotopic vibrational frequencies may be found in the supporting information
[a]See "Theoretical methods" for model and basis set details
[b]Reference [51]
[c]Reference [52]
[d]Reference [53]
[e]Reference [54]

Results and discussion

Peroxides and peroxyl radicals

ROOH and ROO• structures were optimized at the DFT, MP2, and CCSD levels using the basis set described in the "Theoretical methods" section. Structural data and homoisotopic vibrational frequencies for all molecules may be found in the supporting information. Tables 1 and 2 list the heteroisotopic frequencies at the various levels of theory and the difference between them. Clearly the environments of the O_2 fragments in both sets of molecules are highly asymmetric, both from an electronegativity standpoint and from the standpoint of the mass to which they are connected. Moreover, the character of the O–O bond ranges from essentially that of a single bond in the ROOH species to nearly that of molecular oxygen in the halogen atom complexes (the experimental [50] vibrational frequency of O_2 is 1,549 cm^{-1} and the measured [51–54] ^{16}O–^{16}O stretching frequencies in the ROO• molecules range from 1,441 to 1,494 cm^{-1}).

In spite of these asymmetries, however, the data in Tables 1 and 2 illustrate that the O–O stretching frequencies for the two possible heteroisotopomers are in every case quite similar to one another. The absolute difference between the two values is typically from 2 to 3 cm^{-1}. Resolving such a difference is not trivial experimentally—at least for condensed-phase measurements—and indeed for the three cases for which experimental data are available, FOO•, ClOO•, and BrOO•, only for the case of ClOO• has such resolution been accomplished (and in that case DFT agrees closely with experiment). One would conclude from this analysis that observing different frequencies for different O_2 heteroisotopomers might be more the exception than the rule, in the absence of fragment interactions in metal–O_2 complexes significantly different from those manifest in these simple model systems. [As a technical aside, we note that in the ROOH molecules there is generally good agreement between the various levels of theory, with DFT and CCSD being somewhat more robust than MP2 (presumably because of the well-known poor quality of the HF reference for peroxides [31, 55]). In the ROO• molecules, DFT continues to be robust (as judged by comparison with experimental vibrational frequencies—for a much more detailed analysis of DFT applied to these halogen oxides see Ref. [56]), while MP2 and CCSD degrade significantly, again owing to a poor-quality HF wave function that now also includes nontrivial spin contamination. Finally, we note that

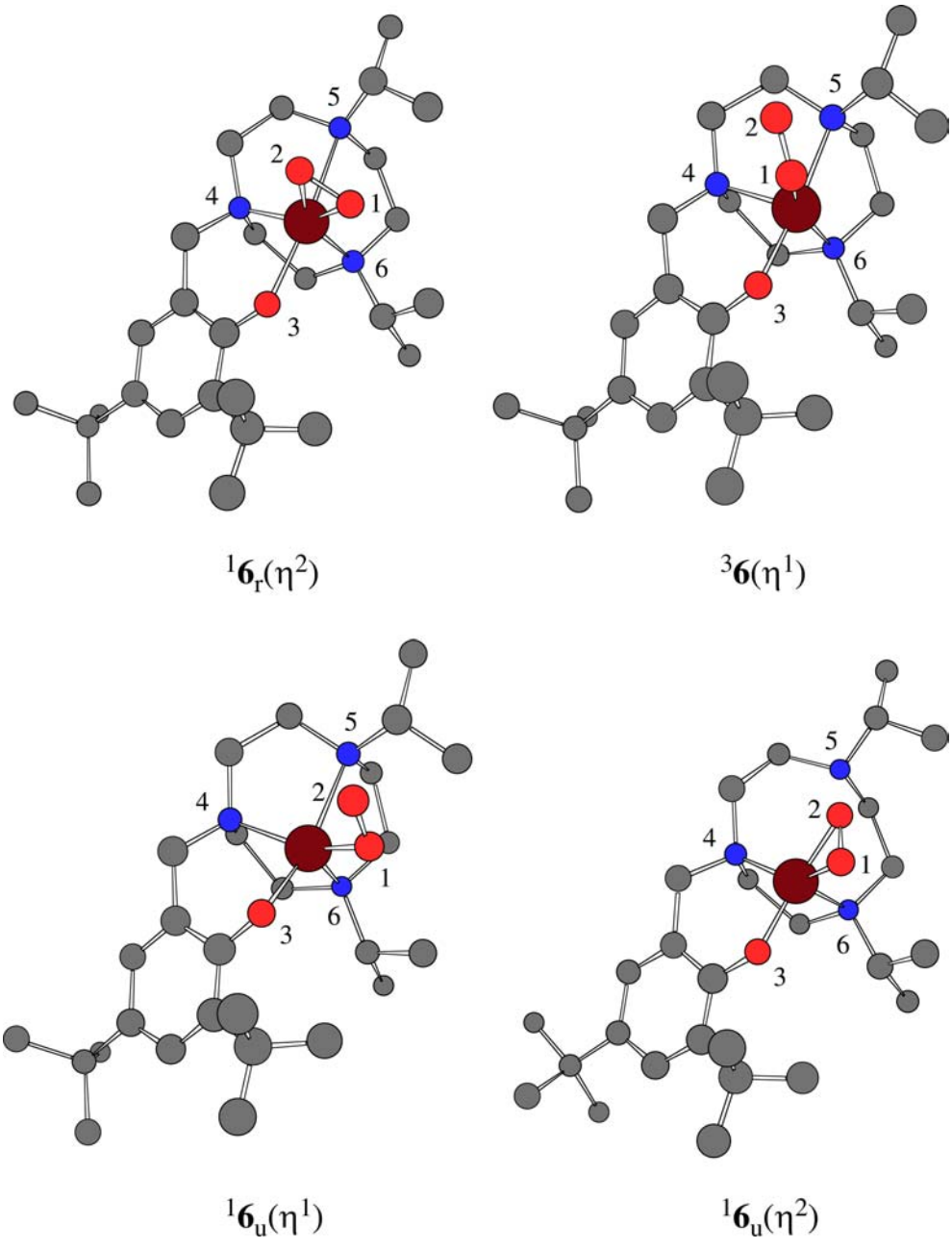

Fig. 1 Stereostructures for stationary points of **6**. Hydrogen atoms have been removed for clarity; copper atoms are *brown*, oxygen atoms *red*, nitrogen atoms *blue*, and carbon atoms *gray*. Atom numbering is for use in Table. 3, 4, 5, and 6

vibrational anharmonicity, which is not explicitly accounted for here, might be expected to change the absolute magnitudes of the fundamental frequencies, but should have negligible effect on the isotopomeric splitting.]

Structures and vibrational frequencies of **6**

Optimization of the geometry of **6** was carried out at the DFT level for both the singlet and the triplet electronic states, although experiment is unambiguous in establishing the singlet as the ground state on the basis of the absence of an electron-spin-resonance spectrum [30]. The triplet state is found to have a single minimum-energy structure and that structure coordinates O_2 in an end-on fashion [$^3\mathbf{6}(\eta^1)$, Fig. 1]. The situation for the singlet state is considerably more complicated. When restricted DFT is employed, the only stable structure is one exhibiting side-on coordination of O_2, namely, $^1\mathbf{6}_r(\eta^2)$, where the "r" subscript in the nomenclature emphasizes the use of restricted DFT. The restricted Kohn–Sham wave function for this structure is unstable to spin-symmetry breaking, however. When such symmetry breaking is permitted through the use of *un*restricted DFT, optimization leads smoothly from $^1\mathbf{6}_r(\eta^2)$ to a structure coordinating O_2 in an end-on fashion, $^1\mathbf{6}_u(\eta^1)$ (where the "u" subscript now indicates unrestricted DFT). When η^2 coordination is enforced in a *partial* optimization at the

Table 3 Selected bond lengths (Å) and CuOO valence bond angles (°) for optimized structures of **6**

Geometry	$^1\mathbf{6}_r(\eta^2)$	$^1\mathbf{6}_u(\eta^2)$	$^1\mathbf{6}_u(\eta^1)$	$^3\mathbf{6}(\eta^1)$
Bond lengths				
O^1O^2	1.378	1.354	1.308	1.297
CuO^1	1.900	1.964	1.966	2.009
CuO^2	1.920	1.964	2.678	2.861
CuO^3	2.224	1.927	2.018	2.023
CuN^4	1.994	2.072	2.082	2.150
CuN^5	2.708	3.377	2.437	2.272
CuN^6	2.075	2.308	2.264	2.181
Bond angle				
CuO^1O^2	69.6	69.8	108.0	118.2

Cartesian coordinates for all structures are provided in the supporting information.

Table 4 Computed isotopomeric O–O vibrational frequencies (cm^{-1}) for optimized structures of **6**

Isotopomer[a]	$^1\mathbf{6}_r(\eta^2)$	$^1\mathbf{6}_u(\eta^2)$	$^1\mathbf{6}_u(\eta^1)$	$^3\mathbf{6}(\eta^1)$	Expt.
$^{16}O^{16}O$	1,007	1,055	1,163	1,191	1,120
$^{16}O^{18}O$	976	1,025	1,120, 1,139[d]	1,159	1,093
$^{18}O^{16}O$	976	1,025	1,121, 1,140[d]	1,159	1,093
$^{18}O^{18}O$	948	996	1,093	1,118	1,059
$\Delta\nu_{mix}$[b]	0	0	1	0	0
$\Delta\nu_{homo}$[c]	59	59	70	73	61

[a]In each case the oxygen atoms are listed as O^1O^2 as defined in Fig. 1.
[b]Frequency difference between the mixed isotopomers
[c]Isotope shift between $^{16}O^{16}O$ and $^{18}O^{18}O$
[d]The O–O stretching mode in this case couples strongly with an aromatic ring deformation so that two bands having roughly equal contributions from both modes are predicted.

unrestricted DFT level, the nitrogen atom of the triazacyclononane ring originally axially coordinated to copper *de*coordinates (although the nitrogen lone pair remains directed towards the copper atom); subsequent full optimization leads to a structure that maintains the side-on coordination mode for O_2, $^1\mathbf{6}_u(\eta^2)$, although the orientation of the O_2 fragment is rotated compared with that in $^1\mathbf{6}_r(\eta^2)$. It is noteworthy that Schatz et al. [26] observed exactly the same phenomenon in their DFT studies of **5**: in order to go from η^1 to η^2 coordination, one nitrogen atom of the tris(tetramethylguanidino)tren ligand had to be permitted to decoordinate. Key geometric details for all structures of **6** are provided in Table 3. Computed O–O stretching frequencies for these structures are listed in Table 4. For now, we postpone a discussion of energetics.

The geometric data are not particularly remarkable, although some trends merit discussion. The coordination of N^5, which is the triazacyclononane nitrogen atom coordinated apically and *trans* to the phenoxide oxygen, is rather weak in every case, at least as judged by the CuN bond distance. That distance grows longer when the O_2 moiety is coordinated side-on, and indeed the CuN bond may be considered to be completely dissociated in $^1\mathbf{6}_u(\eta^2)$. There is also considerable variation in the OO bond length as a function of hapticity and spin state. The bond is longest in the restricted singlet $^1\mathbf{6}_r(\eta^2)$ at 1.378 Å, 0.024 Å shorter in the unrestricted η^2 structure, and about 0.05 Å shorter still in the singlet and triplet η^1 structures.

The computed vibrational frequencies track the bond length predictions in the expected manner, with frequencies for the "normal" isotopomer ranging from 1,007 to 1,191 cm^{-1}. Comparison of computed with experimental O–O stretching frequencies presents something of a puzzle, however. First, there is the issue that in $^1\mathbf{6}_u(\eta^1)$ there is a strong coupling between the O–O stretching mode and an aromatic ring deformation so that two peaks with equal O–O stretching character are predicted for the mixed isotopomer. However, such a coupling is very sensitive to subtle features in the normal mode analysis, and it is entirely possible that factors like solvation or slight variations in the theoretical model would remove this coupling. As such, the only feature that we consider worth interpretation in this instance is that the predicted frequencies for the two mixed isotopomers differ by no more than 1 cm^{-1}. Indeed, a difference in excess of this 1-cm^{-1} value is not predicted for *any* structure. Thus, the failure to observe a mixed-isotope splitting in the experimental RR spectrum does not appear to be diagnostic for a particular O_2 coordination motif.

If we next examine agreement between the absolute theoretical predictions and the experimental measurement for the $^{16}O^{16}O$ isotopomer, there is marginally better agreement between the predicted value for $^1\mathbf{6}_u(\eta^1)$, with an error of $+43$ cm^{-1}, than there is for $^1\mathbf{6}_u(\eta^2)$, with an error of -65 cm^{-1}. On the other hand, if we focus on the full isotope shift on going from $^{16}O^{16}O$ to $^{18}O^{18}O$, we find that this effect is overestimated by 9 cm^{-1} for $^1\mathbf{6}_u(\eta^1)$ but underestimated by only 2 cm^{-1} for $^1\mathbf{6}_u(\eta^2)$. The data for $^1\mathbf{6}_r(\eta^2)$ are in very poor agreement with experiment, which

Table 5 Effects of nitrogen nuclear charges (au) on CuOO valence bond angles (°) and mixed-isotopomer stretching frequencies (cm^{-1}) in optimized structures of $^1\mathbf{8}_u(\eta^1)$

Nuclear charges[a]			∠CuOO	$\nu^{16}O^{18}O$[b]	$\nu^{18}O^{16}O$[b]	$\Delta\nu_{mix}$[c]
N^4	N^5	N^6				
Reference (standard charges)						
7.0	7.0	7.0	114.7	1,153	1,154	1
Increasing molecular charge						
7.1	7.1	7.1	115.5	1,167	1,168	1
7.2	7.2	7.2	117.0	1,184	1,185	1
7.3	7.3	7.3	121.0	1,208	1,209	1
7.4	7.4	7.4	122.1	1,224	1,225	1
Constant neutral charge						
7.0	6.4	7.6	115.0	1,133	1,134	1
7.0	6.3	7.7	122.4	1,089	1,089	0
7.0	6.2	7.8	123.6	1,073	1,073	0
7.0	6.1	7.9	124.4	1,058	1,059	0
7.0	6.0	8.0	125.0	1,033	1,033	0

[a]Nitrogen numbering is the same as that presented in Fig. 1
[b]In each case the oxygen atoms are listed as O^1O^2 as defined in Fig. 1.
[c]Frequency difference between the mixed isotopomers

Table 6 Normal and mixed-isotopomer stretching frequencies (cm^{-1}) in structures of $^1\mathbf{8}_u(\eta^1)$ optimized subject to constrained CuOO valence bond angles (°)

∠CuOO	$\nu^{16}O^{16}O$[a]	$\nu^{16}O^{18}O$[a]	$\nu^{18}O^{16}O$[a]	$\Delta\nu_{mix}$[b]
114.7 (relaxed)	1,187	1,153	1,154	1
135.0	1,202	1,166	1,169	3
150.0	1,220	1,186	1,187	1
165.0	1,255	1,219	1,216	−3
179.0	1,264	1,228	1,225	−3

[a]In each case the oxygen atoms are listed as O^1O^2 as defined in Fig. 1.
[b]Frequency difference between the mixed isotopomers

Table 7 Experimental and theoretical O–O stretching frequencies (cm^{-1}) for **3** and **3a**, respectively

Molecule	$\nu^{16}O^{16}O$	$\nu^{16}O^{18}O$	$\nu^{18}O^{16}O$	$\nu^{18}O^{18}O$
3 (expt.)	1,270	1,241	1,230	1,200
3a (theor.)	1,290	1,255	1,253	1,216

For purposes of isotope identification, the oxygen atoms are listed in the order proximal to cobalt, then distal.

is not particularly surprising given the instability of the restricted Kohn–Sham wave function.

In order to proceed further, it seems necessary to address the question of relative energetics for the various predicted structures. First, however, it is interesting to examine the question of whether a significant difference in mixed isotopomer stretching frequencies can be generated within the general context of the present copper–ligand system. To that end we consider compound **8**, which is found to have a minimum $^1\mathbf{8}_u(\eta^1)$ entirely analogous to $^1\mathbf{6}_u(\eta^1)$. By adjusting the nitrogen nuclear charges and reoptimizing the geometry, one can vary the O–O bond length over the range 1.276–1.341 Å and the CuOO bond angle over the range 114.7–125.0°. In no instance is a mixed-isotopomer splitting of more than 1 cm^{-1} predicted (Table 5). To access a greater range of asymmetric coordination, we then carried out partial optimizations of $^1\mathbf{8}_u(\eta^1)$ (with normal nitrogen nuclear charges) constraining the bond angle to various values extending to 179°. Frequency calculations were then carried out using the method of Baboul and Schlegel [57] to project out contributions from the constrained coordinate. At the very largest bond angles, a mixed-isotopomer splitting of 3 cm^{-1} is predicted (Table 6). Such a splitting is potentially resolvable with an instrument of high resolution under favorable experimental conditions but, like the data presented before for halogen hydroperoxides and haloperoxyl radicals, these results suggest that mixed-isotopomer splittings for O–O vibrations may in general be rather difficult to observe even in highly asymmetric systems.

This observation begs the question of why Proniewicz et al. [23] were able to observe a mixed-isotopomer splitting of 11 cm^{-1} in **3**: what makes this compound so different from all of the others in its sensitivity to isotope position? In order to try to glean insight into this question, we carried out analogous broken-symmetry DFT calculations on an analog of **3** constructed by replacing the mesityl groups with H atoms (**3a**; as the *o*-methyl groups on the mesityl substituents prevent the substituted aromatic ring from conjugating well with the porphyrin, this is a reasonably conservative substitution). Interestingly, DFT predictions for the O–O stretching frequencies of the $^{16}O^{16}O$ and $^{18}O^{18}O$ isomers of **3a** are in fairly good agreement with the observed frequencies for **3** (Table 7). The full isotope shift is also fairly well reproduced. However, DFT predicts a much smaller mixed-isotopomer splitting (2 cm^{-1}) than that observed experimentally. The experimental assignment of the mixed-isotopomer bands is complicated in as much as both are assigned as shoulders on a porphyrin deformation band. If the theoretical model is to be believed, noting that it works well for the experimentally characterized chloroperoxyl radicals, then it may be that the larger splitting reported in the experimental system derives from an effect not present in the computational model, for example, a Fermi resonance or some interaction with the frozen oxygen matrix in which the experiment is performed. Given the nature of the experiment, this system is not likely to be the best one within which to seek a definitive answer of the exact magnitude of the isotopomer splitting in **3**, but the computation is provocative to the extent that it once

Table 8 Relative energies (kcal mol^{-1}) and $\langle S^2\rangle$ values (unitless) of **6** at different *unrestricted* density functional theory levels

Level of theory	$^1\mathbf{6}_r(\eta^2)$	$^1\mathbf{6}_u(\eta^2)$[a]	$^1\mathbf{6}_u(\eta^1)$	$^3\mathbf{6}(\eta^1)$
*m*PWPW91	0.3 (0.549)[b]	0.0 (0.610)	−5.9 (0.997)	−10.3 (2.005)
Sum method[c]	0.1	0.0	−2.6	−10.2
B3LYP//*m*PWPW91[d]	1.7 (0.457)	0.0 (0.565)	−12.4 (1.004)	−14.5 (2.010)
Sum method[c]	0.4	0.0	−12.8	−17.8
B3LYP	3.1 (0.000)	0.0 (0.552)	−12.4 (1.005)	−17.1 (2.010)
Sum method[c]	0.2	0.0	−12.6	−20.0

[a]Electronic energies (E_h) for this column are −1,643.520 96, −1,643.520 98, −1,643.597 83, −1,643.592 66, −1,643.600 79, and −1,643.596 19. These data together with $\langle S^2\rangle$ permit computation of all other electronic energies in the table.
[b]Values in *parentheses* are $\langle S^2\rangle$. Note that in some cases $\langle S^2\rangle \neq 0$ for $^1\mathbf{6}_r(\eta^2)$ because only the *geometry* of this species was computed using restricted density functional theory.
[c]Singlet energies computed from Eq. 1
[d]B3LYP calculations at the *m*PWPW91 geometries

again suggests that such mixed-isotopomer splittings may in general be rather small and difficult to observe.

Relative energetics of **6**, **7**, and **9** at various theoretical levels

The relative energies of the four structures of **6** are reported in Table 8 for the *m*PWPW91 level at which they were optimized. Two sets of relative energies are presented. The first ignores the substantial amount of contamination from the $S_z = 0$ triplet state that affects the various Kohn–Sham wave functions to different degrees. The second applies the sum method of Ziegler et al. [58] to derive ostensibly pure singlet state energies based on the formula [59–61]

$$E_{\text{singlet}} = \frac{2E_{\langle s_z\rangle=0} - \langle S^2\rangle E_{\langle s_z\rangle=2}}{2 - \langle S^2\rangle}, \quad (1)$$

where the triplet energy is computed for the single-determinantal high-spin configuration $S_z = 2$ and $\langle S^2\rangle$ is the expectation value of the total spin operator applied to the Kohn–Sham determinant for the unrestricted $S_z = 0$ calculation. There is debate in the literature regarding the degree to which $\langle S^2\rangle$ provides a quantitative measure of spin contamination in DFT [62–64], but to the extent that the Cu(II)-superoxide mesomer of **6** may be regarded as a disjoint biradical (consistent with $\langle S^2\rangle = 1$) it seems clear that the two different approaches for calculating relative energies may be considered to represent bounds associated with the density functional formalism. Values of $\langle S^2\rangle$ are also listed in Table 8.

When biradical character is present, hybrid density functionals (i.e., those incorporating HF exchange) tend to be more energetically sensitive to spin-symmetry breaking. In the particular case of *X*OO compounds, Filatov and Cremer [56] have argued that hybrid functionals are more appropriate for use with symmetry-broken unrestricted DFT because this avoids a double-counting of nondynamical correlation effects that arises with pure functionals [65–67]. Thus, Table 8 also lists energies computed for the various *m*PWPW91 structures of **6** at the B3LYP level using the same basis set. Note that the predicted relative energies of the end-on and side-on structures are substantially different with the two different functionals, primarily because B3LYP predicts the triplet state to be stabler than the singlet state by roughly twice as much as the pure DFT *m*PWPW91 functional. We have noted elsewhere the tendency for B3LYP to be in error with respect to the ground-state spin for monocopper dioxo species because of multireference character in the singlet state(s) [28, 29], and this is yet another example.

Nevertheless, to check whether or not there might be some artifact associated with the *m*PWPW91 structures discussed thus far, we reoptimized all of the geometries at the B3LYP level. The structures all changed rather little: as a result of optimization each singlet dropped in energy relative to its *m*PWPW91 starting structure by about 2 kcal mol^{-1} and the triplet dropped by 4 kcal mol^{-1} (key geometric data may be found in the supporting information, Table S3; between the two sets of structures the unsigned deviation averaged over all bond lengths listed in Tables 6 and S3 was 0.037 Å). Frequency calculations at the B3LYP level, scaled by a factor of 0.975 to account for the 20% HF exchange in the hybrid functional [33], gave results that were qualitatively similar to those at the *m*PWPW91 level: (1) the experimental frequency is bracketed by those predicted for $^1\mathbf{6}_u(\eta^1)$ (above) and $^1\mathbf{6}_u(\eta^2)$ (below), (2) the predicted frequencies for $^3\mathbf{6}_u(\eta^1)$ and $^1\mathbf{6}_r(\eta^2)$ are substantially larger and smaller, respectively, than experiment, (3) the difference between the $^{16}O^{18}O$ and $^{18}O^{16}O$ isotopomers is never more than 1 cm^{-1}, and (4) the doubly labeled isotope shift predicted for $^1\mathbf{6}_u(\eta^2)$ and $^1\mathbf{6}_r(\eta^2)$ is in close agreement with experiment, while those predicted for $^1\mathbf{6}_u(\eta^1)$ and $^3\mathbf{6}_u(\eta^1)$ are substantially too large. Full details are provided in the supporting information.

In any case, there does not appear to be any particular bias in the *m*PWPW91 structures or energetics compared with those for the B3LYP functional (this provides an interesting contrast to an earlier study of Szilagyi et al. [68], who found that predicted structural and spectroscopic properties of $CuCl_4^{2-}$ improved considerably with increasing HF exchange in the hybrid B3LYP functional compared with the pure BP86 functional). Thus, to the extent that the energetic data in Table 8 may be interpreted, it would appear that the two η^2 structures, which have similar values of $\langle S^2\rangle$, must be regarded as being

Table 9 Relative energies (kcal mol^{-1}) and $\langle S^2\rangle$ values (unitless) of **7** at different theoretical levels

Level of theory	$^1\mathbf{7}_r(\eta^2)$	$^1\mathbf{7}_u(\eta^2)$[a]	$^1\mathbf{7}_u(\eta^1)$	$^3\mathbf{7}(\eta^1)$
*m*PWPW91	−0.5 (0.567)[b]	0.0 (0.639)	−4.7 (0.915)	−10.8 (2.005)
Sum method[c]	−0.8	0.0	0.4	−11.0
CASPT2//*m*PWPW91[d]	−8.5	0.0	15.8	7.6

[a] Electronic energies (E_h) for this column are −1,172.095 65, −1,172.095 30, and −2,626.133 85. These data together with $\langle S^2\rangle$ permit computation of all other electronic energies in the table.
[b] Values in *parentheses* are $\langle S^2\rangle$. Note that $\langle S^2\rangle \neq 0$ for $^1\mathbf{7}_r(\eta^2)$ at the *m*PWPW91 level because only the *geometry* of this species was computed using restricted density functional theory. For complete-active-space calculations, all states are proper spin eigenfunctions.
[c] Singlet energies computed from Eq. 1
[d] CASPT2 calculations at the *m*PWPW91 geometries

fairly close to one another in energy (although every calculation predicts the unrestricted geometry to be slightly lower in energy than the restricted one) in spite of their significant structural dissimilarities. However, given the degree to which the multideterminantal character of the singlet wave functions of **6** renders other energetic comparisons unreliable at the density functional level, we turned instead to multireference second-order perturbation theory (CASPT2) to provide a rigorous description of the different electronic states. [The utility of the restricted-ensemble Kohn–Sham (REKS) method [69] was also examined, but this level incorrectly predicts the triplet to be the ground state by a still larger margin than unrestricted DFT (M. Filatov, personal communication) and we did not consider it further.]

Each structure of **6** contains 82 atoms, making the molecule too large for practical CASPT2 calculations with a reasonably sized basis set. In order to render the system more tractable, we considered instead the 46-atom reduced structures **7**, generated as described in the "Theoretical methods" section. As shown in Table 9, the relative energies of **7** are for the most part rather similar to those for **6** at the DFT level—the largest change is that the energy of the η^1 singlet increases by 3 kcal mol^{-1} relative to the energy of the η^2 singlet—suggesting that **7** is an acceptable model for **6**. The active space employed in the

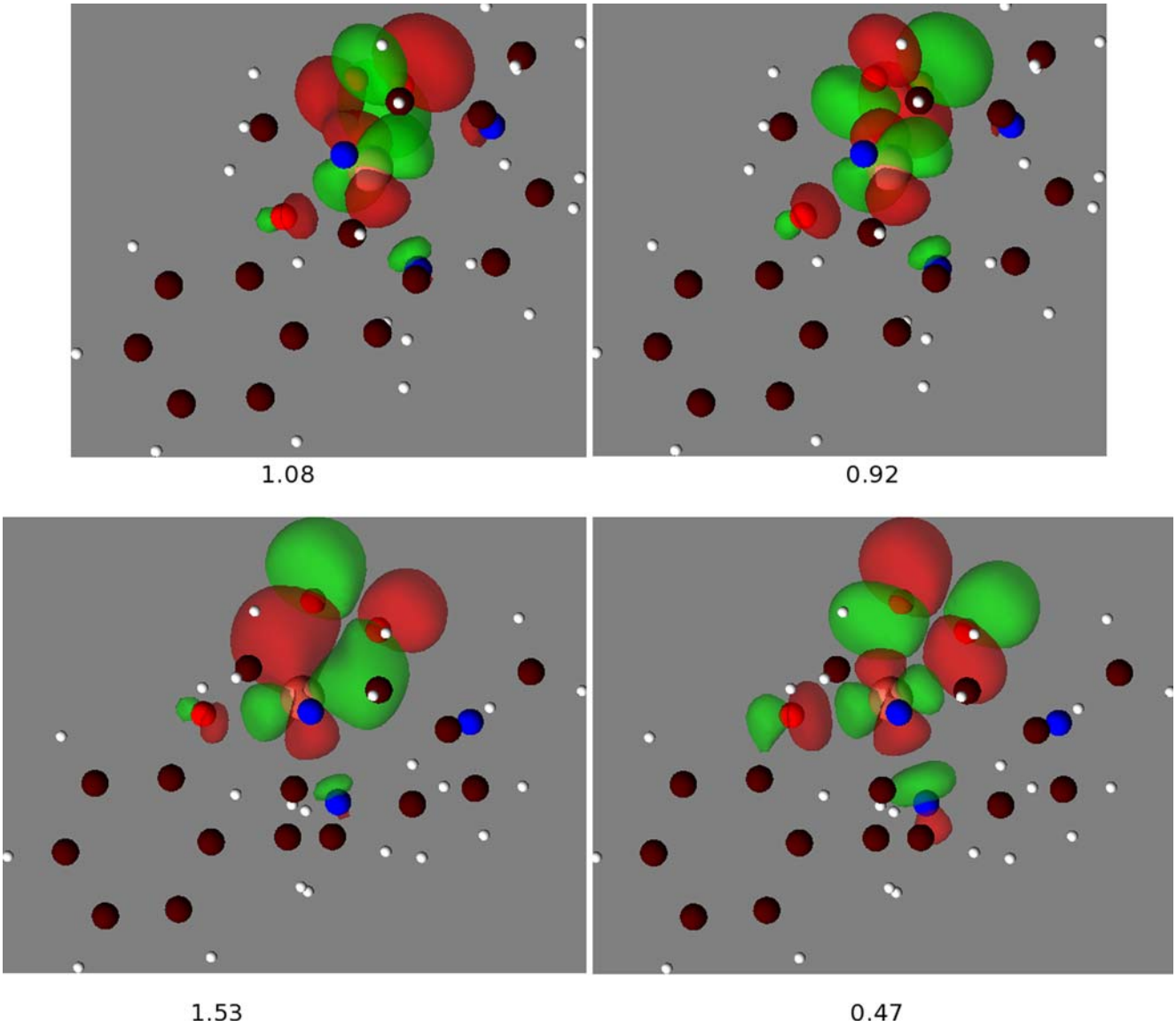

Fig. 2 Frontier orbitals with occupation numbers for $^1\mathbf{7}_u(\eta^2)$ (*lower*) and $^1\mathbf{7}_u(\eta^1)$ (*upper*). Hydrogen, carbon, nitrogen, oxygen, and copper atoms are represented by *white*, *brown*, *blue*, *red*, and *golden spheres* (without explicit bonds), respectively. In each case, the two orbitals differ essentially only in the phase of combination between the Cu *d* orbital and the overlapping O_2 π^* orbital. Thus, as the occupation numbers more nearly approach 1.0, the system corresponds more closely to a disjoint Cu(II)-superoxide-like singlet biradical

CAS calculations was of size (12,12), constructed from the six highest energy occupied orbitals and the six lowest energy virtual orbitals. This active space was chosen from considering the convergence behavior of CAS(n, n) calculations for various values of n on the smaller model system **9** derived from extreme truncation of **6**. Data from these calculations together with comparisons of different basis sets (since **9** is so small, it permits the use of more complete basis sets) may be found in the supporting information.

The CASPT2/BS3 method predicts that singlet structure $^1\mathbf{7}_r(\eta^2)$ is the lowest in energy by 8.5 kcal mol^{-1} compared with the next-nearest singlet structure $^1\mathbf{7}_u(\eta^2)$, and by 16.1 kcal mol^{-1} compared with $^3\mathbf{7}(\eta^1)$. The prediction of a singlet ground state is consistent with experiment. The large difference in relative energetics between CASPT2 and DFT, with the former providing agreement with experiment for the correct ground state while the latter fails to do so, is consistent with past experience regarding Cu–O_2 adducts [28, 29]. Analysis of the results for **9** suggests that deficiencies in basis-set and active-space size may lead to errors as large as 4–5 kcal mol^{-1} in predicted relative energies for **7**; however, the qualitative ordering of the relative energies noted before are invariant to errors of this magnitude.

With respect to the key nondynamical correlation present in the singlet structures of **7**, the two CASSCF orbitals that show occupation numbers most significantly different from 2 and 0 correspond closely to the nominal highest occupied molecular orbital and the lowest unoccupied molecular orbital at the HF and DFT levels, and these orbitals are depicted in Fig. 2 for the η^1 and η^2 bonding motifs. Each case, as expected [16, 28, 29, 70], involves the bonding and antibonding combinations of an O_2 π^* orbital with the most strongly overlapping Cu d orbital. In structures $^1\mathbf{7}_r(\eta^2)$ and $^1\mathbf{7}_u(\eta^2)$, the occupation numbers of the lower- and higher-energy orbitals are nearly the same, about 1.55 and 0.45, respectively [the precise values for $^1\mathbf{7}_u(\eta^2)$ are in Fig. 2]. These occupation numbers reflect the relative weighting of the two closed-shell determinants that differ in which of the two orbitals is doubly occupied, these weights being about 0.66 and 0.20, respectively, which represents a decidedly nontrivial degree of biradical character. The analogous orbitals in $^1\mathbf{7}_u(\eta^1)$ have occupation numbers of 1.08 and 0.92, respectively, and the corresponding configuration-state-function weights are 0.46 and 0.40, which indicates an essentially perfect biradical. The wave function for $^3\mathbf{7}_u(\eta^1)$ is well represented by a single (high-spin) determinant and has occupation numbers of 1.0 and 1.0 for the frontier orbitals.

From a technical standpoint, the CASPT2 results help to rationalize the trends observed in the DFT energies. The moderate biradical character in the η^2 structures causes them to be poorly treated at the Kohn–Sham level compared with the single-determinantal triplet, so that the energy of the triplet relative to the energies of the η^2 singlets is estimated to be unrealistically low (indeed, so low as to be the ground state). Since the DFT energy for $^1\mathbf{7}_u(\eta^1)$ is derived from a density that formally represents a 50:50 mixture of the singlet and triplet states, this energy too is predicted to be anomalously stable compared with the energies of the η^2 singlets. The use of the sum method *does* cause the energy of $^1\mathbf{7}_u(\eta^1)$ relative to that of $^3\mathbf{7}_u(\eta^1)$ to be predicted in semiquantitative agreement with the CASPT2 results, as expected for a case where the singlet and triplet have spatially similar orbitals [58]. In the case of the η^2 singlets, the sum method fails to provide similar accuracy because the level of biradical character is only moderate—enough to cause the Kohn–Sham formalism to be unstable, but not so much as to cause the singlet and triplet wave functions to be characterized by substantially similar spatial orbitals.

In any case, if we take the CASPT2 data for **7**, and adjust those data for changes on going from **7** to **6** computed at the DFT level, our best energetic prediction is that structure $^1\mathbf{6}_r(\eta^2)$ represents the global minimum on the ground-state surface by 7.6 kcal mol^{-1}, with the next-lowest-energy isomer being $^1\mathbf{6}_u(\eta^2)$. This energy separation is only slightly outside the rough error estimate we have arrived at on the basis of calculations on **9**, so it is probably dangerous to insist on the former being stabler than the latter, but what seems very clear is that the oxygen coordination is predicted to be η^2. This is also consistent with the isotope shifts predicted for $^1\mathbf{6}_r(\eta^2)$ and $^1\mathbf{6}_u(\eta^2)$ both being in good agreement with experiment even though the absolute frequencies deviate by 70–110 cm^{-1}. We note at this point that we have ignored the effects of solvation in all of our calculations, although the experiment is conducted in solution. However, we expect the solvation free energies of the various isomers to differ by considerably less than the error already introduced into the gas-phase theoretical models by the biradical character of the complexes, so that our qualitative conclusions with respect to the minimum-energy geometry remain unchanged.

It is, of course, somewhat disappointing that a single level of electronic structure theory does not appear to be capable of simultaneously optimizing molecular geometries, computing relative energies, and predicting vibrational frequencies. Nevertheless, we consider the theoretical evidence in toto to provide strong support for a side-on oxygen coordination motif in **6**. Jazdzewski et al. [30] originally proposed a structure for **6** topologically equivalent to that of $^1\mathbf{6}_r(\eta^2)$ in part on the basis of the failure to observe a mixed-isotopomer splitting in the RR spectrum and in part on the basis of the solid intuition inherent in the experimental group. While we have shown the former *not* to be diagnostic of side-on coordination, the latter should certainly never be discounted by theoreticians. Indeed, it must further be acknowledged that in the absence of experimental data with which to compare the various calculations, it would be quite difficult to draw *any* conclusions about structure and energetics even from the state-of-the-art electronic structure methods employed here, thus demonstrating that systems like Cu–O_2 complexes continue to pose significant challenges to modern theory.

Acknowledgements This work was supported by the National Science Foundation (CHE-0203346). Bill Tolman is thanked for stimulating discussions and boundless enthusiasm.

References

1. Klinman JP (1996) Chem Rev 96:2541–2562
2. Kaim W, Rall J (1996) Angew Chem Int Ed Engl 35:43–60
3. Borman CD, Saysell CG, Sokolowski A, Twitchett MB, Wright C, Sykes AG (1999) Coord Chem Rev 192:771–779
4. Whittaker JW (2003) Chem Rev 103:2347–2364
5. Mure M, Mills SA, Klinman JP (2002) Biochemistry 41:9269–9278
6. Klinman JP (2003) Biochim Biophys Acta 1647:131–137
7. Stewart LC, Klinman JP (1988) Annu Rev Biochem 57:551–590
8. Eipper BA, Stoffers DA, Mains RE (1992) Annu Rev Neurosci 15:57–85
9. Eipper BA, Milgram SL, Husten EJ, Yun HY, Mains RE (1993) Protein Sci 2:489–497
10. Prigge ST, Kolhekar AS, Eipper BA, Mains RE, Amzel LM (1997) Science 278:1300–1305
11. Prigge ST, Mains RE, Eipper BA, Amzel LM (2000) Cell Mol Life Sci 57:1236–1259
12. Prigge ST, Eipper BA, Mains RE, Amzel LM (2004) Science 304:864–867
13. Lewis EA, Tolman WB (2004) Chem Rev 104:1047–1076
14. Mirica LM, Ottenwaelder X, Stack TDP (2004) Chem Rev 104:1013–1045
15. Vaska L (1976) Acc Chem Res 9:175–183
16. Solomon EI, Tuczek F, Root DE, Brown CA (1994) Chem Rev 94:827–856
17. Weitzer M, Schindler S, Brehm G, Schneider S, Hormann E, Jung B, Kaderli S, Zuberbuhler AD (2003) Inorg Chem 42:1800–1806
18. Fujisawa K, Tanaka M, Moro-oka Y, Kitajima N (1994) J Am Chem Soc 116:12079–12080
19. Chen P, Root DE, Campochiaro C, Fujisawa K, Solomon EI (2003) J Am Chem Soc 125:466–474
20. Kurtz DM, Shriver DF, Klotz IM (1976) J Am Chem Soc 98:5033–5035
21. Klotz IM, Kurtz DM (1984) Acc Chem Res 17:16–22
22. Shiemke AK, Loehr TM, Sanders-Loehr J (1984) J Am Chem Soc 106:4951–4956
23. Proniewicz LM, Kulczycki A, Weselucha-Birczynska A, Majcherczyk H, Nakamoto K (1999) New J Chem 23:71–76
24. Nakamura A, Tatsuno Y, Yamamoto M, Otsuka S (1971) J Am Chem Soc 93:6052–6058
25. Chaudhuri P, Hess M, Weyhermüller T, Wieghardt K (1999) Angew Chem Int Ed Engl 38:1095–1098
26. Schatz M, Raab V, Foxon SP, Brehm G, Schneider S, Reiher M, Holthausen MC, Sundermeyer J, Schindler S (2004) Angew Chem Int Ed Engl 43:4360–4363
27. Cramer CJ, Tolman WB, Theopold KH, Rheingold AL (2003) Proc Natl Acad Sci USA 100:3635–3640
28. Gherman BF, Cramer CJ (2004) Inorg Chem 43:7281–7283
29. Aboelella NW, Kryatov S, Gherman BF, Brennessel WW, Young VG, Sarangi R, Rybak-Akimova E, Hodgson KO, Hedman B, Solomon EI, Cramer CJ, Tolman WB (2004) J Am Chem Soc 126:16896–16911
30. Jazdzewski BA, Reynolds AM, Holland PL, Young VG, Kaderli S, Zuberbuhler AD, Tolman WB (2003) J Biol Inorg Chem 8:381–393
31. Hehre WJ, Radom L, Schleyer PvR, Pople JA (1986) Ab initio molecular orbital theory. Wiley, New York
32. Schwerdtfeger P, Szentpaly Lv, Vogel K, Silberbach H, Stoll H, Preuss H (1986) J Chem Phys 84:1606–1612
33. Cramer CJ (2004) Essentials of computational chemistry, 2nd edn. Wiley, Chichester
34. Adamo C, Barone V (1998) J Chem Phys 108:664–675
35. Perdew JP, Wang Y (1986) Phys Rev B 33:8800–8802
36. Perdew JP (1991) In: Ziesche P, Eschrig H (eds) Electronic structure of solids '91. Akademie Verlag, Berlin, pp 11–20
37. Møller C, Plesset MS (1934) Phys Rev 46:618–622
38. Purvis GD, Bartlett RJ (1982) J Chem Phys 76:1910–1918
39. Stevens WJ, Krauss M, Basch H, Jasien PG (1992) Can J Chem 70:612–629
40. Becke AD (1988) Phys Rev A 38:3098–3100
41. Lee C, Yang W, Parr RG (1988) Phys Rev B 37:785–789
42. Becke AD (1993) J Chem Phys 98:5648–5652
43. Stephens PJ, Devlin FJ, Chabalowski CF, Frisch MJ (1994) J Phys Chem 98:11623–11627
44. Andersson K, Malmqvist P-Å, Roos BO (1992) J Chem Phys 96:1218–1226
45. Dolg M, Wedig U, Stoll H, Preuss H (1987) J Chem Phys 86:866–872
46. Roos BO, Lindh R, Malmqvist P-Å, Veryazov V, Widmark P-O (2004) J Phys Chem A 108:2851–2858
47. Karlström G, Lindh R, Malmqvist P-Å, Roos BO, Ryde U, Veryazov V, Widmark PO, Cossi M, Schimmelpfennig B, Neogrady P, Seijo L (2003) Comput Matl Sci 28:222–239
48. Roos BO, Taylor PR, Siegbahn PEM (1980) Chem Phys 48:157–173
49. Frisch MJ, Trucks GW, Schlegel HB, Scuseria GE, Robb MA, Cheeseman JR, Montgomery JA, Vreven T, Kudin KN, Burant JC, Millam JM, Iyengar SS, Tomasi J, Barone V, Mennucci B, Cossi M, Scalmani G, Rega N, Petersson GA, Nakatsuji H, Hada M, Ehara M, Toyota K, Fukuda R, Hasegawa J, Ishida M, Nakajima T, Honda Y, Kitao O, Nakai H, Klene M, Li X, Knox JE, Hratchian HP, Cross JB, Adamo C, Jaramillo J, Gomperts R, Stratmann RE, Yazyev O, Austin AJ, Cammi R, Pomelli C, Ochterski JW, Ayala PY, Morokuma K, Voth GA, Salvador P, Dannenberg JJ, Zakrzewski VG, Dapprich S, Daniels AD, Strain MC, Farkas O, Malick DK, Rabuck AD, Raghavachari K, Foresman JB, Ortiz JV, Cui Q, Baboul AG, Clifford S, Cioslowski J, Stefanov BB, Liu G, Liashenko A, Piskorz P, Komaromi I, Martin RL, Fox DJ, Keith T, Al-Laham MA, Peng CY, Nanayakkara A, Challacombe M, Gill PMW, Johnson B, Chen W, Wong MW, Gonzalez C, Pople JA (2003) Gaussian 03 (Revision B.05). Gaussian, Inc., Pittsburgh
50. Andrews L, Smardzewski RR (1973) J Chem Phys 58:2258–2261
51. Misochko EY, Akimov AV, Wight CA (1999) J Phys Chem A 103:7972–7977
52. Jacox ME (1980) J Mol Spectrosc 84:74–88
53. Arkell A, Schwager I (1967) J Am Chem Soc 89:5999–6006
54. Tevault DE, Smardzewski RR (1978) J Am Chem Soc 100:3955–3957
55. Dixon DA, Andzelm J, Fitzgerald G, Wimmer E (1991) J Phys Chem 95:9197–9202
56. Filatov M, Cremer D (2003) Phys Chem Chem Phys 5:2320–2326
57. Baboul AG, Schlegel HB (1997) J Chem Phys 107:9413–9417
58. Ziegler T, Rauk A, Baerends EJ (1977) Theor Chim Acta 43:261–271
59. Yamaguchi K, Jensen F, Dorigo A, Houk KN (1988) Chem Phys Lett 149:537–542
60. Lim MH, Worthington SE, Dulles FJ, Cramer CJ (1996) In: Laird BB, Ross RB, Ziegler T (eds) Chemical applications of density functional theory. American Chemical Society, Washington, DC, pp 402–422
61. Isobe H, Takano Y, Kitagawa Y, Kawakami T, Yamanaka S, Yamaguchi K, Houk KN (2002) Mol Phys 100:717–727
62. Pople JA, Gill PMW, Handy NC (1995) Int J Quantum Chem 56:303–305
63. Gräfenstein J, Cremer D (2001) Mol Phys 99:981–989
64. Clark AE, Davidson ER (2002) J Phys Chem 106:6890–6896
65. Polo V, Kraka E, Cremer D (2002) Theor Chem Acc 107:291–303
66. Cremer D, Filatov M, Polo V, Kraka E, Shaik S (2002) Int J Mol Sci 3:604–638

67. Gräfenstein J, Kraka E, Filatov M, Cremer D (2002) Int J Mol Sci 3:360–394
68. Szilagyi RK, Metz M, Solomon EI (2002) J Phys Chem A 106:2994–3007
69. Filatov M, Shaik S (1999) Chem Phys Lett 304:429–437
70. Aboelella NW, Lewis EA, Reynolds AM, Brennessel WW, Cramer CJ, Tolman WB (2002) J Am Chem Soc 124:10660–10661